

2021-07

Using time series of MODIS land surface phenology to model temperature and photoperiod controls on spring greenup in North American deciduous forests

M. Moon, B. Seyednasrollah, A.D. Richardson, M.A. Friedl. 2021. "Using time series of MODIS land surface phenology to model temperature and photoperiod controls on spring greenup in North American deciduous forests." *Remote Sensing of Environment*, Volume 260, pp. 112466 - 112466. <https://doi.org/10.1016/j.rse.2021.112466>

<https://hdl.handle.net/2144/45104>

"Downloaded from OpenBU. Boston University's institutional repository."

1 **Using Time Series of MODIS Land Surface Phenology to Model Temperature and**
2 **Photoperiod Controls on Spring Greenup in North American Deciduous Forests**

3

4

5 Minkyu Moon^{1*}, Bijan Seyednasrollah^{2,3}, Andrew D. Richardson^{2,3}, Mark A. Friedl¹

6

7 ¹Department of Earth and Environment, Boston University

8 ²School of Informatics, Computing, and Cyber Systems, Northern Arizona University

9 ³Center for Ecosystem Science and Society, Northern Arizona University

10 *Corresponding author: 685 Commonwealth Avenue, Boston, MA 02215, USA

11 E-mail address: moon.minkyu@gmail.com (Minkyu Moon)

12

13 **Abstract**

14 The timing of leaf emergence in temperate and boreal forests is changing, which has
15 profound implications for a wide array of ecosystem processes and services. Spring phenology
16 models, which have been widely used to predict the timing of leaf emergence, generally assume
17 that a combination of photoperiod and thermal forcing control when leaves emerge. However,
18 the exact nature and magnitude of how photoperiod and temperature individually and jointly
19 control leaf emergence is the subject of ongoing debate. Here we use a continuous development
20 model in combination with time series of land surface phenology measurements from MODIS to
21 quantify the relative importance of photoperiod and thermal forcing in controlling the timing of
22 canopy greenup in eastern temperate and boreal forests of North America. The model accurately
23 predicts biogeographic and interannual variation in the timing of greenup across the study region
24 (median RMSE = 4.6 days, median bias = 0.30 days). Results reveal strong biogeographic
25 variation in the period prior to greenup when temperature and photoperiod influence greenup that
26 covaries with the importance of photoperiod versus thermal controls. Photoperiod control on leaf
27 emergence is dominant in warmer climates, but exerts only modest influence on the timing of
28 leaf emergence in colder climates. Results from models estimated using ground-based
29 observations of cloned lilac are consistent with those from remote sensing, which supports the
30 realism of remote sensing-based models. Overall, results from this study suggest that apparent
31 changes in the sensitivity of trees to temperature are modest and reflect a trade-off between
32 decreased sensitivity to temperature and increased photoperiod control, and identify a transition
33 in the relative importance of temperature versus photoperiod near the 10 °C isotherm in mean
34 annual temperature. This suggests that the timing of leaf emergence will continue to move earlier

35 as the climate warms, and that the magnitude of change will be more pronounced in colder
36 regions with mean annual temperatures below 10 °C.

37 **Keywords:** spring phenology, climate change, deciduous forests, photoperiod, temperature
38 sensitivity, Bayesian, hierarchical modeling, MODIS, land surface phenology

39

40 **1. Introduction**

41 There is overwhelming evidence that leaf emergence is occurring earlier in temperate and
42 boreal forests (Menzel et al., 2006; Schwartz et al., 2006). However, a number of recent papers
43 have concluded that the sensitivity of leaf emergence to changes in temperature has decreased in
44 recent decades (Fu et al., 2015; Piao et al., 2017) and that the period when trees are sensitive to
45 thermal forcing is becoming shorter (Fu et al., 2019; Güsewell et al., 2017; Wenden et al., 2020).
46 These results complicate interpretation of observed trends and exacerbate challenges involved in
47 forecasting how the phenology of trees will change in the future. These challenges are further
48 complicated by fundamental issues in the way that the sensitivity of phenological events to
49 temperature is generally quantified (Keenan et al., 2019). Because changes in phenology impact
50 important ecosystem functions (Keenan et al., 2014; Richardson et al., 2013), understanding how
51 changes in climate affect phenology is critical to forecasting how ecosystems will respond to
52 future climate change (Peñuelas et al., 2009; Piao et al., 2019).

53 To address this, a variety of recent studies have focused on improving understanding of
54 bioclimatic controls on plant phenology (Liu et al., 2017; Zohner et al., 2016). Results from both
55 lab- and field-based experimental studies have provided insights (Montgomery et al., 2020;
56 Richardson et al., 2018a), but are limited by the fact that phenological behavior in controlled
57 laboratory- and field-based warming experiments differs from behavior observed in natural
58 ecosystems (Clark et al., 2014a; Wolkovich et al., 2012). Further, the manner in which
59 environmental conditions are perturbed in such experiments (e.g., 2 °C warming) is not
60 representative of climate changes expected in the future, which are predicted to occur gradually,
61 but with large year-to-year variability (Schewe et al., 2019; Walther et al., 2002). These issues
62 are compounded by the fact that the geographic sampling of data sets used in these studies is

63 often limited and does not reflect the full biogeographic range of species examined (Richardson
64 et al., 2013). Hence, geographic variation in the relative importance of different climate drivers
65 on phenology, both within and across plant communities, is not well understood (Piao et al.,
66 2019).

67 One widely used strategy for investigating the response of plant phenology to climate change
68 is to calibrate mechanistic models using weather data in combination with long-term records of
69 phenology collected on the ground (Basler, 2016; Fu et al., 2019) or from remote sensing (Liu et
70 al., 2017; Melaas et al., 2018). In addition to thermal controls, photoperiod is widely assumed to
71 control the timing of leaf emergence by regulating the entrance of ecodormancy, triggering
72 thermal forcing to stimulate bud swelling and leaf emergence (Chuine et al., 2016; Jackson, 2009;
73 Körner and Basler, 2010). Hence, many models include explicit representation of photoperiod
74 (e.g., Blümel and Chmielewski, 2012; Masle et al., 1989; Basler, 2016; Migliavacca et al., 2012).
75 To capture the role of thermal forcing, mechanistic models generally use aggregated bioclimatic
76 variables such as growing degree days or winter chilling as their primary inputs. However, Clark
77 et al. (2014a) have suggested that the use of such aggregated quantities is problematic because
78 values for prescribed variables required by these models (e.g., start date of forcing accumulation)
79 are not identifiable.

80 In recent years, data-driven models based on state-space representations of phenological
81 processes have been developed that overcome many of the weaknesses of both mechanistic and
82 experimental approaches (e.g., Clark et al., 2014b; Qiu et al., 2020; Senf et al., 2017;
83 Seyednasrollah et al., 2018). By modeling phenological dynamics directly from data, these
84 models avoid issues arising from misspecification of functional relationships between forcing
85 variables and processes that regulate phenological development (Clark et al., 2014b). Building on

86 this approach, here we use a data-driven spring onset model in combination with gridded weather
87 data and time series of ground-based and remotely sensed observations of spring greenup dates
88 to explore biogeographic patterns in photoperiod and thermal controls on the timing of spring
89 greenup. Specifically, we use this model to : (1) quantify the relative importance of thermal
90 forcing, photoperiod, and winter chilling in controlling spring greenup; (2) identify the pre-
91 season period when plants are sensitive to bioclimatic controls; and (3) characterize how
92 covariance among thermal forcing, photoperiod, and the length of the pre-season period control
93 the biogeography of spring greenup in deciduous forests of eastern temperate and boreal North
94 America.

95

96 **2. Methods**

97 **2.1. Study Region**

98 The study region includes the Northern Forests and Eastern Temperate Forest ecoregions
99 included in level 1 of the US EPA Ecoregions of North America (Fig. A1). To distinguish
100 deciduous forests from evergreen forests and other land cover types within the study area, the
101 500 m Collection 6 MODIS Land Cover Type product was used. This product provides annual
102 land cover maps based on machine learning that are post-processed using a multi-temporal state-
103 space modeling framework that reduces spurious land cover change introduced by classification
104 uncertainty in individual years (Abercrombie and Friedl, 2016; Sulla-Menashe et al., 2019).

105 The continuous development spring onset model (Section 2.3) is estimated on an equal-area
106 grid, where each grid cell is 4.67 km x 4.67 km (10×10 MODIS pixels; ~ 22 km²). In each grid
107 cell, only pixels labeled as deciduous broadleaf or mixed forests throughout the entire study
108 period from 2001-2017 were included in the analysis. To ensure analyses were based on grid

109 cells dominated by deciduous forest cover, we excluded model grid cells where the fraction of
110 MODIS pixels labeled as deciduous broadleaf or mixed forests was less than 50% (Fig. A1).

111

112 **2.2. Spring Greenup and Meteorological Data**

113 To identify the timing of springtime leaf emergence from 2001 to 2017, we used the
114 Collection 6 MODIS Land Cover Dynamics product (MCD12Q2; Gray et al., 2019). This
115 product uses time series of the two-band Enhanced Vegetation Index (EVI2) to identify the
116 timing of six key phenophase transition dates during each growing season in each 500-m MODIS
117 pixel. Numerous studies have reported that this product provides a reliable measure of vegetation
118 phenology (Moon et al., 2019; Richardson et al., 2018b) and seasonal changes in ecological
119 function and surface biophysical characteristics (Melaas et al., 2013; Moon et al., 2020). For this
120 analysis, we use the MCD12Q2 ‘greenup’ metric, which is defined by the Land Cover Dynamics
121 product as the day of year (DOY) during the greenup phase in spring when the EVI2 time series
122 at each pixel crosses 15% of its seasonal amplitude (Gray et al., 2019).

123 To provide the meteorological data required for model estimation, we used the Version 3
124 Daymet dataset for North America (Thornton et al., 2017) (<https://daymet.ornl.gov>). This data
125 set uses digital elevation data in association with a land-water mask and meteorological
126 observations collected at ground-based stations to create gridded time series of surface
127 meteorological fields at daily time step and 1 km spatial resolution for the period 1980 to present.
128 For this work, we used daily maximum and minimum 2-m air temperatures from 2000 to 2017
129 along with daylength, resampled to 500 m and co-registered to the MODIS data over all grid
130 cells included in our analysis.

131

132 **2.3. Continuous Development Spring Onset Model**

133 To estimate the sensitivity of different climatological controls on springtime phenology, we
134 developed a continuous development spring onset model (hereafter, CDSOM) based on a
135 hierarchical Bayesian framework that predicts the timing of springtime greenup using three
136 drivers: photoperiod, thermal forcing, and chilling units. The original form of this model was
137 proposed by Clark et al. (2014b), who used the same general approach to show that because
138 conventional process-based phenology models (e.g., Hufkens et al., 2018.) aggregate daily air
139 temperature time series into cumulative sums or mean values for each year or season, they
140 misrepresent how thermal forcing controls the timing of phenology.

141 Similar to Clark et al. (2014b), the CDSOM we use here tracks the continuous response of
142 phenological development to variation in environmental controls at daily time step. To do this,
143 the model uses a state-space framework that includes an unobservable latent state (h), which
144 responds continuously to environmental controls and captures ecological responses to
145 bioclimatic forcing:

$$h_{g,s,d+1} = h_{g,s,d} + \delta h_{g,s,d} \quad (1)$$

146 where $h_{g,s,d}$ is the latent state for grid cell g and sample (i.e., pixel) s on day d . In this framework,
147 $\delta h_{g,s,d}$ is the increment in h from day d to day $d + 1$, which is estimated using:

$$\delta h_{g,s,d} = \begin{cases} (X_{g,s,d} \times \beta_g)(1 - h_{g,s,d}/h_{max}), & \delta h_{g,s,d} \geq 0 \\ 0, & \delta h_{g,s,d} < 0 \end{cases} \quad (2)$$

148 where $X_{g,s,d}$ is a matrix of predictor variables that includes the daily mean temperature ($T_{g,s,d}$),
149 day-length (i.e., photoperiod; $L_{g,s,d}$), and chilling units ($CU_{g,s}$; defined below) on each day, and
150 where daily mean temperature is computed as the average of daily maximum and minimum

151 temperatures from Daymet in each 500 m MODIS pixel. β_g is a vector of estimated model
 152 coefficients for each grid cell (g), and h_{max} is the final state value of h , which is prescribed to be
 153 100. Note that: (1) even though a linear formulation is used to describe the relationship between
 154 model predictors and coefficients, the model accommodates nonlinear responses in phenological
 155 responses to environmental controls using an asymptotic limit for the latent state (i.e., $h_{g,s,d}/$
 156 h_{max}); and (2) the latent state increment is always non-negative.

157 To convert the continuous scale of the latent state (h) into a form that identifies discrete
 158 phenological events (i.e., the timing of spring greenup onset), a logit transformation is used:

$$\text{logit}(P_{g,s,d}) = \kappa + \lambda \times h_{g,s,d} \quad (3)$$

159 where $P_{g,s,d}$ is the probability that the onset occurs at sample pixel s in grid g on day d , and κ and
 160 λ are the intercept and slope of the transformation, respectively. Because greenup onset is
 161 defined to be a discrete event, $P_{g,s,d}$ follows a Bernoulli distribution:

$$Y_{g,s,d} \sim \text{Bernoulli}(P_{g,s,d}) \quad (4)$$

162 where $Y_{g,s,d}$ indicates whether or not greenup onset has occurred for sample s in grid g on day d .

163 Following convention, chilling units ($\text{CU}_{g,s}$) were defined as:

$$\text{CU}_{g,s} = \sum_{d=c_{g,0}}^{c_{g,s}} I(T_{g,s,d} < T_b) \quad (5)$$

164 Hence, $\text{CU}_{g,s}$ is defined as the number of days below prescribed threshold T_b during the period
 165 after the onset of dormancy until an unobserved date $c_{g,s}$ when the chilling requirement is
 166 satisfied. Previous studies have suggested that boreal and temperate tree species respond to air

167 temperatures ranging from -5 to 10 °C as a threshold for chilling requirements (Hänninen et al.,
168 2019). Here we used 0 °C because the study area covers a large range of climate conditions.
169 Further, and more importantly, sensitivity analyses revealed that model results were not sensitive
170 to variation in T_b (not shown), which is supported by results indicating that chilling control on
171 the timing of greenup is minor (see Results).

172

173 **2.4. CDSOM Estimation**

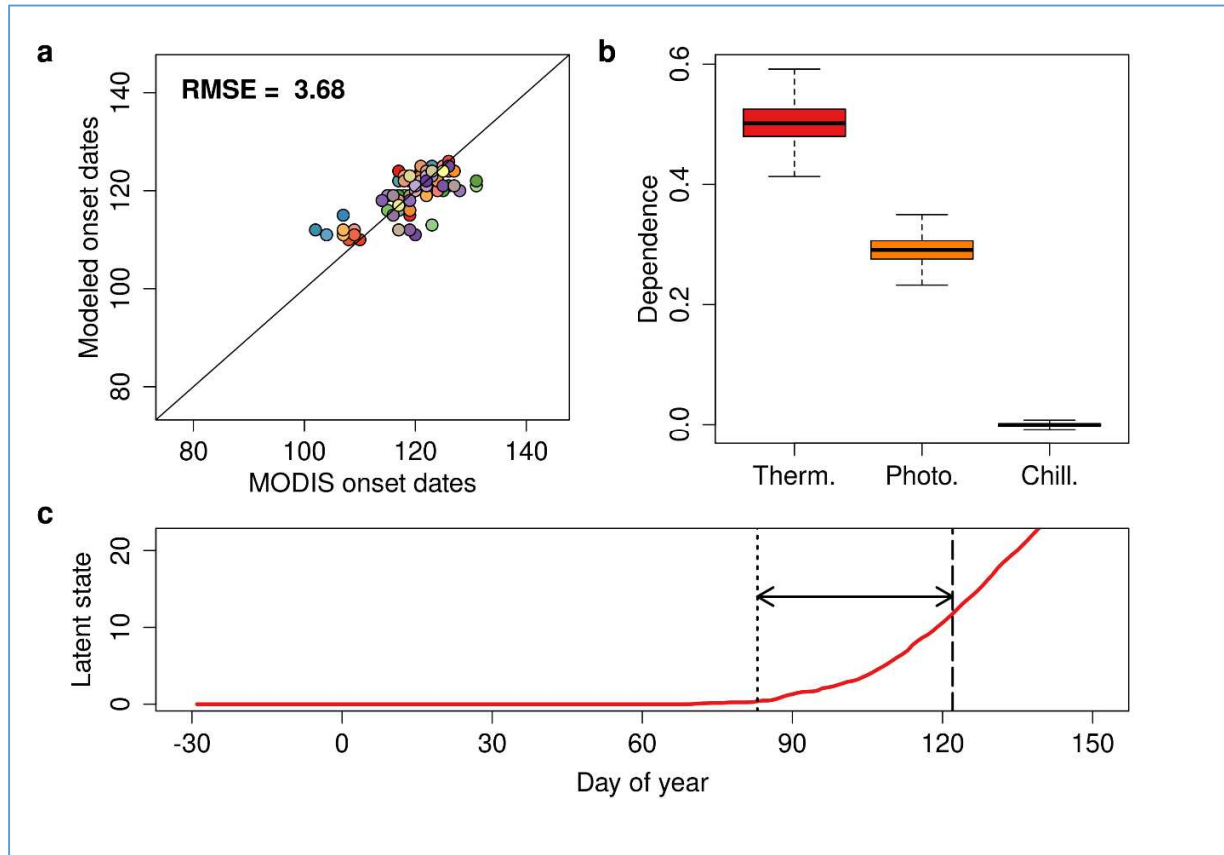
174 As we described above, the CDSOM was estimated using a regular grid, with each grid
175 cell composed of 100 MODIS pixels. We excluded all pixels with more than one land cover type
176 label between 2001 and 2017 (i.e., that nominally experienced change) and excluded all cells that
177 were composed of less than 50% deciduous or mixed forests. Because the CDSOM is
178 computationally expensive, we used a two-stage sampling approach to estimate the model for
179 randomly selected grid cells in each of the 13 MODIS tiles that intersect the study region. In the
180 first stage, we randomly sampled grid cells within each MODIS tile that met the criteria listed
181 above. If less than 300 valid grid cells were available within a tile, we included all valid grid
182 cells. If more than 300 grid cells were available in a tile, we randomly selected a sample of 300
183 cells. In the second stage, we randomly selected MODIS pixels located in each grid cell across
184 time. To minimize the impact of spatial and temporal correlation, we used a sub-sample of 100
185 pixel-years (i.e., 100 unique greenup dates randomly selected across 17 years) to estimate a
186 unique model for each cell. Each sample was selected from a total pool of between 850-1700
187 sample points (i.e., 50-100 pixels per year in each grid across 17 years).

188 For each year, December 1st of the previous year and DOY 250 (~Sept. 7) of the current year
189 were used as the start and end dates of latent state development, respectively. Posterior sampling

190 was performed using the “R2jags” package in R (Su and Yajima, 2015), with 10,000 iterations
191 and 3,000 burn-in periods. As a final step, to reduce noise in our results, we excluded grid cells
192 where estimated model coefficients were outside 95% of the range of estimated model
193 coefficients across all grid cells. This yielded a final data set consisting of 1,685 grid cells with
194 valid results.

195

196 Model results from a representative grid cell are shown in Fig. 1. Overall, predicted onset
197 dates are well aligned with observed onset dates at this grid cell, with a root-mean-square error
198 (RMSE) of 3.7 days across the time series (Fig. 1a). Because the input forcing data are
199 normalized prior to model estimation (i.e., having a mean of 0 and a standard deviation of 1 for
200 each of the input variables in each grid g and sample s), the posterior distributions for each
201 model coefficient, which reflect the dependence of phenological development on each input
202 variable, show differences that are independent of the magnitude or units of each input variable
203 (Fig. 1b). Time series of the latent state generated by the model (Fig. 1c) provide information
204 regarding the timing and duration of the pre-season period prior to greenup onset. This period
205 has been previously described as “as the most temperature-sensitive period preceding the
206 phenological event” (Güsewell et al., 2017) or “the period before leaf unfolding for which the
207 partial correlation coefficient between leaf unfolding and air temperature is highest” (Fu et al.,
208 2015). Here we define this period as corresponding to the time interval when phenological
209 development is affected by bioclimatic forcing, and we use the CDSOM to identify the “pre-
210 season period” as starting on the DOY when the latent state variable (h) starts to increase and
211 ending on the DOY when greenup onset occurs (i.e., the period indicated by the arrow in Fig. 1c).



212

213 **Fig. 1.** Model results for a randomly selected grid cell. (a) Relationship between the greenup
 214 onset dates from MODIS and onset dates estimated by the model. (b) The distribution of model
 215 coefficients for each control variable (i.e., the relative dependence on each climate control;
 216 Therm.: thermal forcing; Photo.: photoperiod; Chill.: chilling units). (c) Time series of the latent
 217 state (red line) and the length of the pre-season (identified by the horizontal arrow). In panel (a),
 218 each dot (total $n = 100$) represents an individual pixel-year sampled from the grid cell comprised
 219 of 10 by 10 MODIS pixels across 17 years of the study period (i.e., 100 out of the total 1,700
 220 pixel-years).

221

222 **2.5. Quantifying the Relative Importance of Bioclimatic Forcing Variables**

223 To address our goal of quantifying the relative importance (and geographic variation thereof)
224 among bioclimatic controls on the timing of springtime phenology, we compute a normalized
225 index with values that range from -1 to +1 that captures this effect. Because each of the input
226 variables in each grid g and sample s have been normalized to have a mean of 0 and a standard
227 deviation of 1, model coefficients can be directly compared to assess the relative importance of
228 each control variable. To quantify this, we calculated the relative importance (RI) of each control
229 variable relative to each other variable using a normalized index computed from CDSOM model
230 results. For example, to compute the relative importance of photoperiod versus thermal forcing
231 in any given grid cell, we computed:

$$RI = \frac{\beta_T - \beta_L}{\beta_T + \beta_L} \quad (6)$$

232 where β_T and β_L are the average model coefficients for thermal forcing and photoperiod
233 (respectively) during the pre-season period, which are estimated for each grid cell by the
234 CDSOM.

235

236 **2.6. CDSOM Assessment and Comparison with Conventional Phenology Models**

237 To provide a baseline comparison against previously developed and widely used springtime
238 phenology models (hereafter, the ‘conventional models’), we compared results from the CDSOM
239 with four widely used process-based phenology models included in the “phenor” package in R
240 (Hufkens et al., 2018). Specifically, we compared our results against the thermal time (TT)
241 model, the photo-thermal time (PTT) model, the exponential photo-thermal time model (M1),
242 and the alternating (AT) model, as described by Hufkens et al. (2018). These models are

243 fundamentally different from the CDSOM in that they assume a linear relationship between
 244 spring thermal forcing and the rate of phenological development, and that spring onset occurs
 245 when accumulated forcing (after a prescribed start date) reaches a critical threshold (F^*). The TT
 246 model relies only on thermal forcing (daily air temperature in each MODIS pixel, $T_{g,s,d}$) with no
 247 additional inputs. In this model, the state of forcing (S_f) increases each day until F^* is reached,
 248 when leaves emerge (Chuine et al., 1999; Hunter and Lechowicz, 1992):

$$R(T_{g,s,d}) = \begin{cases} 0 & \text{for } T_{g,s,d} \leq T_b \\ T_{g,s,d} - T_b & \text{for } T_{g,s,d} \geq T_b \end{cases} \quad (6)$$

$$S_f = \sum_{t_0}^t R(T_{g,s,d}) \quad (7)$$

249 where t_0 is the start date. For consistency with the CDSOM, we set t_0 and T_b to December 1st
 250 and 0 °C, respectively. The PTT model includes day-length (i.e., photoperiod; $L_{g,s,d}$) as an
 251 additional factor that regulates the rate of thermal forcing (Črepinšek et al., 2006; Masle et al.,
 252 1989):

$$S_f = \sum_{t_0}^t R(T_{g,s,d}) \times \frac{L_{g,s,d}}{24} \quad (8)$$

253 The exponential M1 model also includes photoperiod, but treats the relationship between
 254 photoperiod and S_f as an exponential (Blümel and Chmielewski, 2012):

$$S_f = \sum_{t_0}^t R(T_{g,s,d}) \times \left(\frac{L_{g,s,d}}{24} \right)^k \quad (9)$$

255 where k is an empirically estimated constant. Finally, the AT model includes the number of days
 256 when the daily mean temperature falls below T_b (i.e., the number of chilling days; NCD), and

257 treats NCD as an exponential function that reduces the thermal forcing accumulation required for
258 spring onset to occur (Cannell and Smith, 1983):

$$F^* = a + b \times \exp[c \times \text{NCD}(t)] \quad (10)$$

259 where a , b , and c are empirically estimated constants, and $\text{NCD}(t)$ is defined as the number of
260 chilling days since December 1st. A table summarizing the variables and main characteristics of
261 the CDSOM and conventional models is provided as an appendix (Table A1).

262 For this analysis, we assessed model performance for both the CDSOM and the conventional
263 models in two ways. First, we assessed results from model-based predictions for the timing of
264 spring greenup based on all available years (from 2001 to 2017). Second, to provide a more
265 robust assessment of model performance, we held out two years (2010 and 2012) with
266 anomalously warm springs in much of the study region (Friedl et al., 2014), and evaluated model
267 performance for each of these years. In this way, we were able to assess not only how well the
268 models performed under average conditions, but also how well they performed under unusual
269 springtime weather conditions that were not represented in the data used to estimate the models.

270

271 **2.7. CDSOM Estimation Using Ground-Based Observations**

272 As a final element of our analysis, to complement model results based on remotely sensed
273 greenup dates and to provide an independent basis for assessing the realism and robustness of
274 our results, we estimated the CDSOM using time series of leaf unfolding dates for cloned lilac
275 (*Syringa x chinensis* ‘Red Rothomagensis’) (Rosemartin et al., 2015). By applying the model to
276 data from cloned plants, genetic variability is eliminated, and which allows us to investigate how
277 differences in the timing of leaf unfolding between different individuals are caused by

278 differences in local environmental controls. Unlike our approach using MODIS spring greenup
279 dates, the model is estimated by pooling site-years across the region because the number of lilac
280 leaf-out dates for each location is too small to accurately estimate models for each site. The
281 dataset includes 254 leaf unfolding dates from 60 locations across the study region, spanning the
282 period from 2001 to 2008 (Fig. A1). For reasons we explain below, we stratified the dataset into
283 ‘warm’ versus ‘cold’ sites based on whether the mean annual temperature at each site is above or
284 below 10 °C. Based on this stratification, the model was applied to 182 and 72 leaf unfolding
285 dates for the colder and warmer regions, respectively.

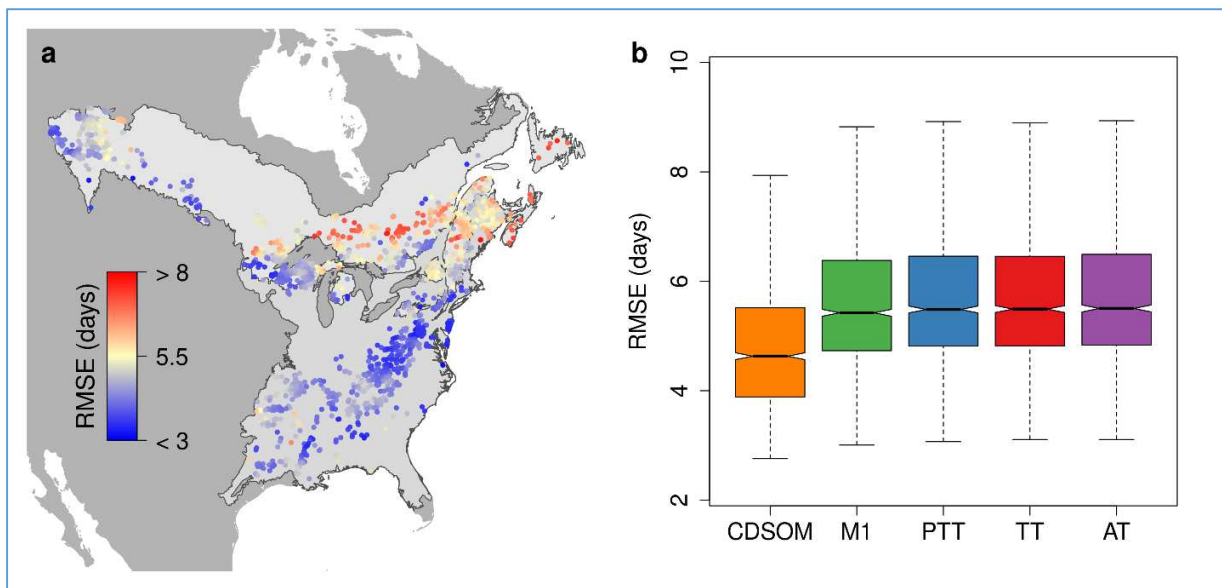
286

287 **3. Results**

288 The CDSOM accurately predicts biogeographic and interannual variation in the timing of
289 springtime greenup across the study region. The median RMSE between predicted and observed
290 spring greenup dates was 4.6 days (Fig. 2), which is roughly equivalent to the uncertainty in
291 spring greenup dates estimated from MODIS (Moon et al., 2019). Inspection of results from the
292 conventional spring onset models show that median RMSEs were ~20% larger (~5.5 days vs. 4.6
293 days) relative to those obtained from the CDSOM (Fig. 2b). Further, RMSEs for years with
294 anomalous springs (2010 and 2012) were unchanged for the CDSOM, but increased by roughly 2
295 days for conventional models when 2010 and 2012 were excluded during model estimation (Fig.
296 3). For completeness, Fig. A2 shows the relationship between anomalies in MODIS greenup
297 dates and anomalies in predicted onset set dates, and demonstrates that the CDSOM outperforms
298 the conventional models in capturing year-to-year variations in spring onset dates. These results
299 suggest that the CDSOM not only provides more accurate predictions of greenup relative to
300 predictions from conventional phenology models, but that the CDSOM more effectively captures

301 the impact of geographic and year-to-year variation in bioclimatic controls. More generally, the
302 accuracy of CDSOM results indicates that the model realistically captures the nature and
303 magnitude of ecophysiological responses to interannual and biogeographic variation in climate
304 controls that regulate the timing of greenup.

305

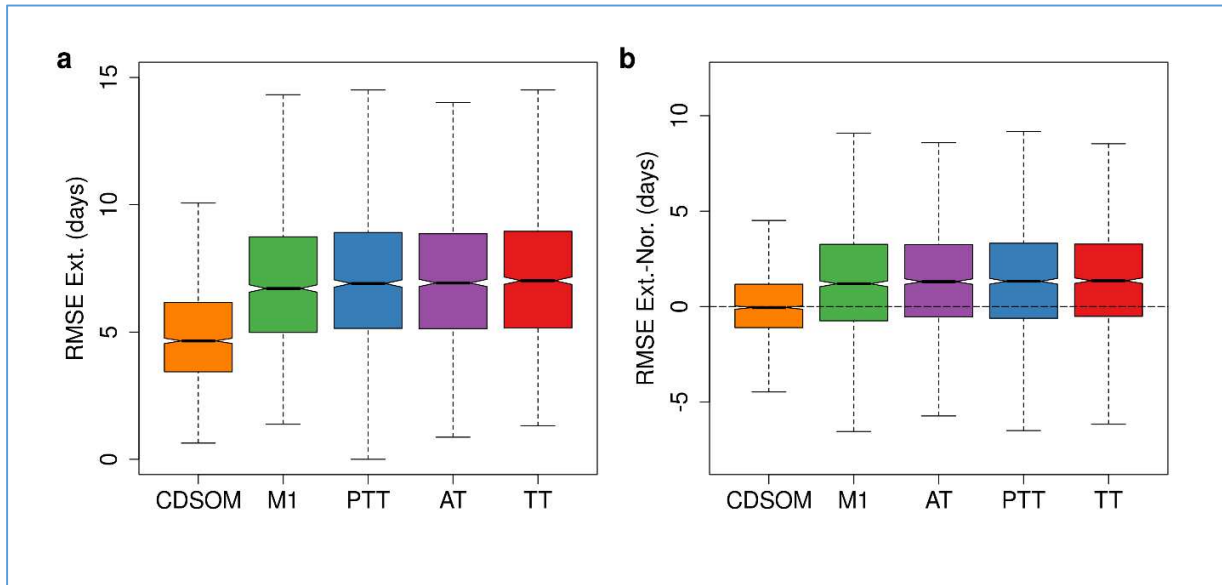


306

307 **Fig. 2.** Continuous Development Spring Onset Model (CDSOM) performance. (a) Geographic
308 variation in model root-mean-square error (RMSE) between greenup onset dates observed from
309 MODIS and onset dates predicted by the CDSOM model. (b) Boxplots showing the distribution
310 of RMSEs for the CDSOM model and four widely used conventional spring greenup models.
311 M1: The exponential photo-thermal time model; PTT: The photo-thermal time model; TT: The
312 thermal time model; AT: The alternating model. In panel (b), boxplots are presented in
313 increasing order of magnitude with respect to mean RMSE.

314

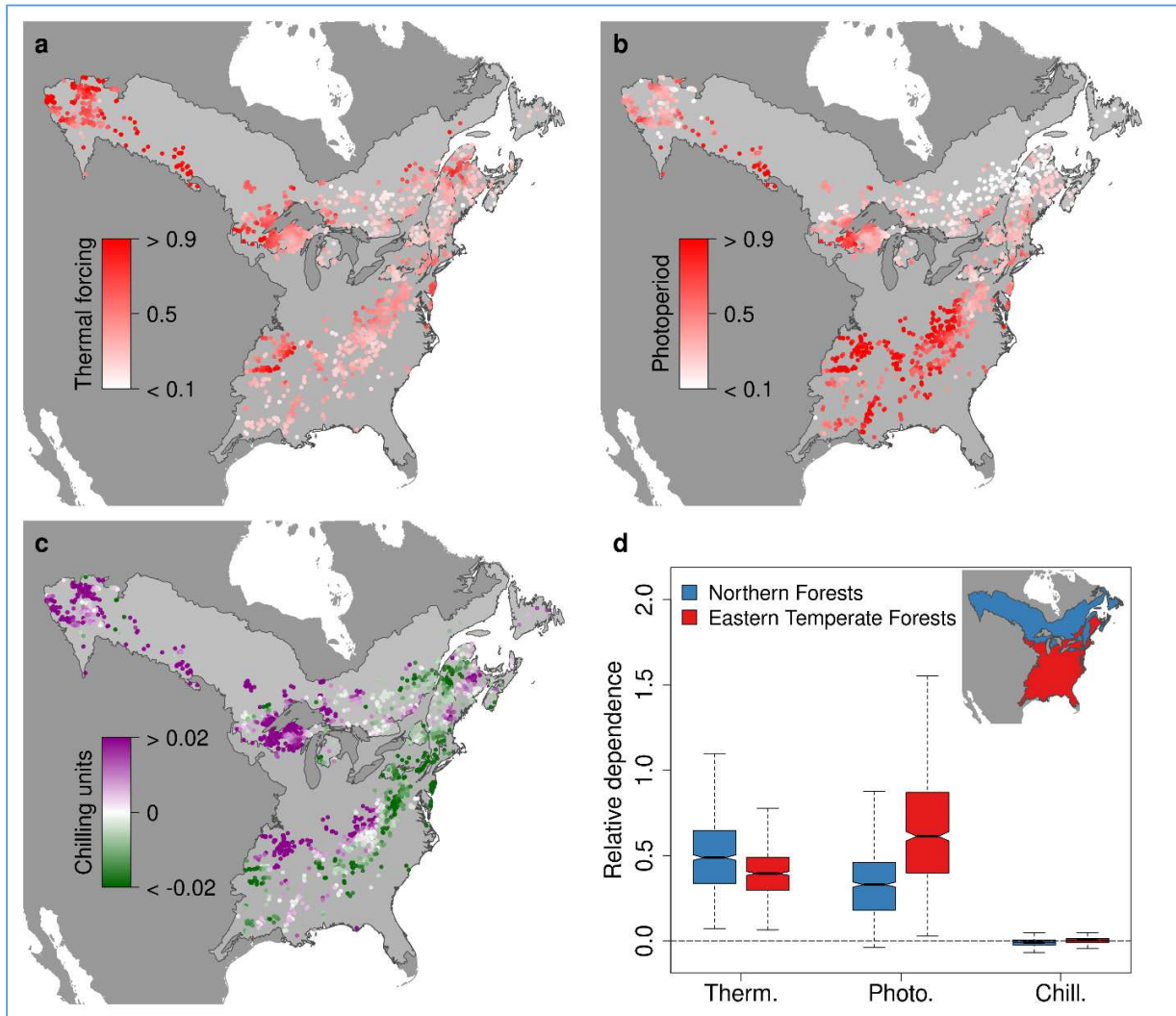
315



316
 317 **Fig. 3.** RMSE results across models for anomalous years. (a) Boxplots of RMSEs for each model
 318 for 2010 and 2012. (b) Boxplots showing increase in RMSEs for model predictions for all years
 319 versus anomalous years (i.e., RMSEs for 2010 and 2012 – RMSEs for 2001-2017) at each grid
 320 cell. CDSOM: continuous development spring onset model; M1: The exponential photo-thermal
 321 time model; PTT: The photo-thermal time model; TT: The thermal time model; AT: The
 322 alternating model. Boxplots are presented in increasing order of magnitude with respect to mean
 323 RMSE.

324

325



326

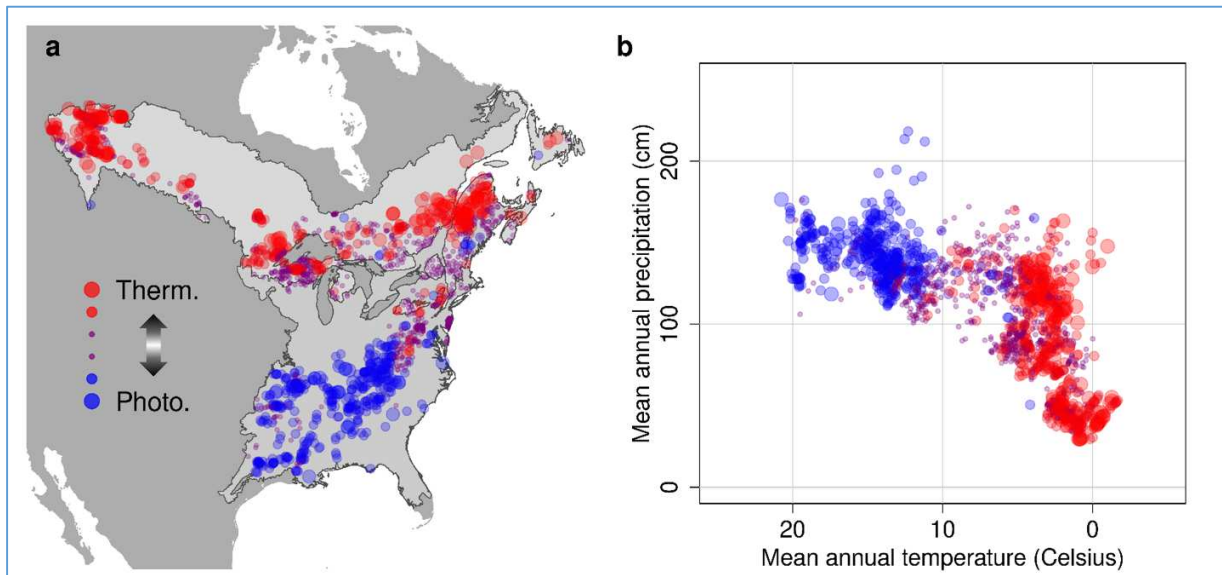
327 **Fig. 4.** Geographic variation in the dependence of spring greenup onset date to: (a) thermal
 328 forcing, (b) photoperiod, and (c) chilling units. In panel (d), boxplots show the distribution of
 329 model coefficients for each control variable during the pre-season period prior to leaf emergence
 330 in Northern Forests (blue) versus Eastern Temperate Forests (red). Differences between the
 331 means in both cases are statistically significant ($p < 0.001$).

332

333 The dependence of spring greenup on thermal forcing estimated by the CDSOM is higher in
334 Northern Forests than in Eastern Temperate forests (Fig. 4), but overall differences, while
335 statistically significant, are modest. In contrast, dependence on photoperiod control exhibits
336 systematic geographic variation across the study domain, with large differences between each
337 ecoregion. Eastern Temperate Forests, which are warmer, show substantially higher dependence
338 on photoperiod relative to the Northern Forests ecoregion, which is much cooler (Fig. 4b and 4d).
339 This difference is especially pronounced in Eastern Canada where dependence on photoperiod is
340 low, versus the Southern United States, where photoperiod dependence is high. Dependence of
341 spring onset on chilling units is uniformly low throughout the study region, which indicates that
342 the influence of chilling control, relative to photoperiod and thermal forcing, is effectively
343 negligible (Fig. 4c and 4d).

344 Geographic patterns in the *RI* of photoperiod versus thermal forcing indicates that
345 photoperiod exerts proportionally more control on the timing of spring greenup in warmer
346 regions, while thermal forcing exerts proportionally more control in colder regions (Fig. 5a). By
347 plotting the *RI* in climate space (i.e., as a function of mean annual temperature and precipitation)
348 (Fig. 5b), the pattern becomes even more clear. In regions where mean annual temperature is
349 above ~10 °C, photoperiod exerts stronger control on the timing of spring greenup than thermal
350 forcing. Conversely, in regions where mean annual temperature is less than ~10 °C, thermal
351 forcing is more important. *RI* values near the 10 °C isotherm in mean annual temperature are
352 generally close to zero, indicating equal influence of thermal forcing and photoperiod (plotted as
353 purple points in Fig. 5). These results suggest that the 10 °C isotherm in mean annual
354 temperature identifies a transition zone between regions where thermal forcing versus
355 photoperiod is more dominant.

356



357

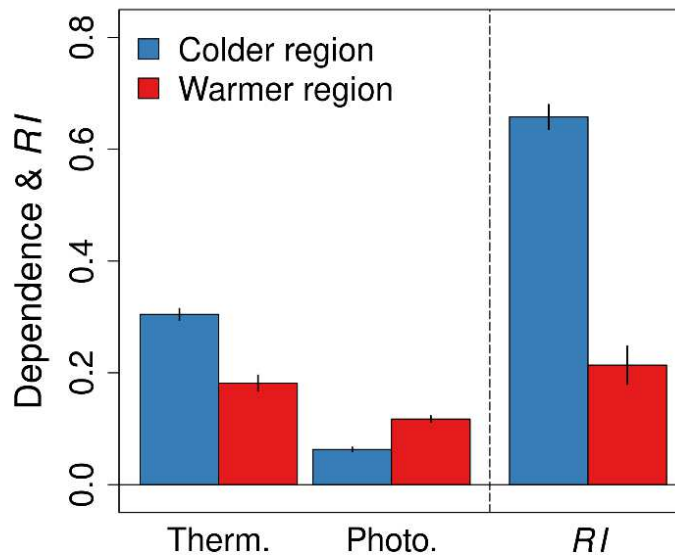
358 **Fig. 5.** Relative importance (*RI*) of thermal forcing versus photoperiod. Circles in red and blue
359 show locations where thermal forcing and photoperiod, respectively, exert stronger control on
360 the timing of spring greenup; purple circles identify locations where the magnitude of thermal
361 forcing and photoperiod are roughly equivalent. The size of each circle is proportional to the
362 magnitude of *RI* in each cell.

363

364 Results from applying CDSOM to ground-based observations of leaf unfolding dates for
365 cloned lilac reveal that even though the individual lilac plants are genetically identical, the
366 relative dependence of leaf unfolding dates on thermal forcing versus photoperiod depends on
367 local bioclimatic conditions (Fig. 6). Consistent with previous studies (Basler and Körner, 2012;
368 Schwartz et al., 2006), model coefficients and *RI* values indicate that leaf unfolding in cloned
369 lilac depends more strongly on thermal forcing than on photoperiod, irrespective of location.
370 However, thermal control is stronger in colder regions and *RI* values are significantly smaller

371 (i.e., thermal control is less dominant) in warm sites than in cold sites. In addition, comparison of
372 cloned lilac data against greenup dates from MODIS for the same location show that MODIS
373 greenup dates are biased late relative to lilac unfolding dates (Fig. A3), especially in warmer
374 areas with earlier greenup dates, which supports the conclusion that lilacs are sensitive to
375 temperature.

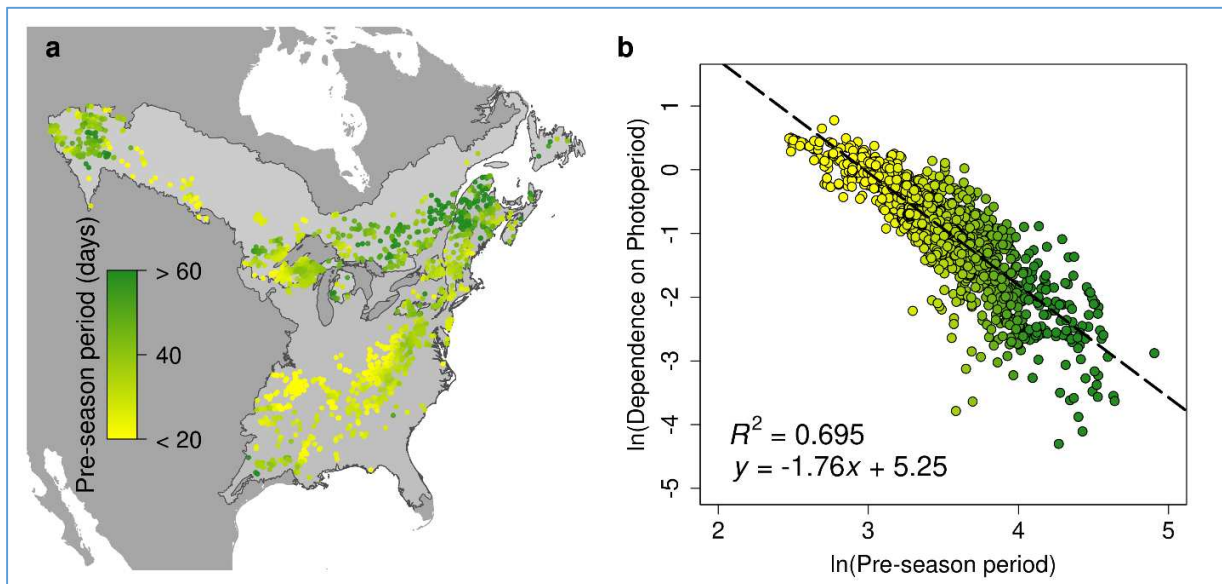
376



377
378 **Fig. 6.** Dependence of cloned lilac leaf unfolding date on thermal forcing and photoperiod, and
379 relative importance (*RI*). 254 total leaf unfolding dates from cloned lilac were divided into two
380 groups based on mean annual temperature (≤ 10 °C, $n = 182$; > 10 °C, $n = 72$). The left panel
381 plots the mean dependence of leaf unfolding on thermal forcing and photoperiod estimated by
382 the CDSOM. The right panel plots the mean *RI* in each group. Positive *RI* indicates stronger
383 control by thermal forcing relative to photoperiod. Vertical lines show ± 1 standard deviation.

384

385 Finally, results from the CDSOM reveal patterns of covariance among pre-season period
386 length, photoperiod, and thermal forcing that jointly control the timing of greenup that are not
387 captured in conventional models. In particular, geographic variation in the pre-season period is
388 strongly and negatively correlated with geographic variation in the relative importance of
389 photoperiod on spring greenup. Fig. 7b shows that this relationship follows a power law, where
390 photoperiod control decreases ($R^2 = 0.70$, $p < 0.001$) as the length of the pre-season period
391 increases. Fig. 7b also reveals modest heteroscedasticity in the relationship between pre-season
392 period length and photoperiod control, which reflects the fact that spring greenup in locations
393 with cooler mean annual temperatures and longer pre-seasons have lower dependence on
394 photoperiod and higher dependence on thermal forcing (Fig. 5). In contrast, the relationship
395 between pre-season period and dependence on thermal forcing is statistically significant, but
396 much weaker ($R^2 = 0.13$; Fig. A4).
397



398

399 **Fig. 7.** Variation in pre-season period and the relationship between greenup dependence on
400 photoperiod and length of pre-season period. (a) Geographic pattern in pre-season period, and (b)
401 log-log relationship between the dependence of greenup on photoperiod and the length of the
402 pre-season period.

403

404 **4. Discussion**

405 We assessed the relative importance of photoperiod, chilling, and thermal forcing in
406 controlling the timing of leaf emergence in Eastern Temperate and Boreal Forest ecoregions of
407 North America. To do this, we used a hierarchical Bayesian model in combination with time
408 series of land surface phenology measurements from remote sensing. The former provides a
409 data-driven framework for investigating how different bioclimatic controls influence the timing
410 of leaf emergence (Clark et al., 2014b; Seyednasrollah et al., 2020); the latter provides a robust
411 and repeatable means of measuring and monitoring phenological dynamics over large areas
412 (Bolton et al., 2020; Zhang et al., 2018).

413 The core hypotheses that motivate this research include two main elements. First, the
414 ecophysiological processes that control leaf emergence respond continuously to variation in
415 environmental controls throughout pre-season period prior to greenup in a manner that is not
416 represented in conventional models (Clark et al., 2014b). Second, rather than simply acting as a
417 cue for entering ecodormancy, photoperiod exerts continuous control on the timing of greenup
418 during the pre-season period. The results presented in this study suggest that both hypotheses are
419 supported. The pre-season period, which corresponds to the period when the CDSOM latent state
420 variable (h) responds to bioclimatic forcing (Fig. 1c), ranges from roughly 2-12 weeks over the
421 study domain (Fig. 7a). Throughout this period, changes in h reflect the net effect of daily

422 changes thermal and photoperiod controls. By estimating the model in a spatially explicit fashion
423 over a large geographic and climatic range, CDSOM results provide an empirical basis for
424 quantifying not only how thermal forcing and photoperiod individually and jointly influence the
425 timing of greenup, but more generally, how the length of the preseason period and relative
426 importance of photoperiod versus thermal forcing vary over the study domain.

427 Conventional models calibrated using long-term observations of phenological events such as
428 those used in this study have been widely used to simulate and forecast phenological events for
429 decades (Chuine and Régnière, 2017). Like the CDSOM, these models generally use air
430 temperature, photoperiod, and chilling units in different configurations and combinations to
431 parameterize the response of plants to bioclimatic controls and predict the timing of phenophase
432 transitions (Basler, 2016; Hufkens et al., 2018). However, as we described previously, Clark et al.
433 (2014a, 2014b) argue that most conventional phenology models are fundamentally limited
434 because: (1) they aggregate measurements with substantial day-to-day variability over periods of
435 weeks-to-months into single parameters and therefore do not capture how short-term variability
436 in control variables influences the timing of leaf emergence; (2) they rely on parameters that are
437 not identifiable; and (3) they do not account for uncertainty in model predictors or leaf
438 emergence data. As a solution, Hänninen et al. (2019) argue that carefully designed factorial
439 experiments provide the most robust basis for improving understanding of processes that control
440 leaf emergence, and hence, for developing and testing process-based models. However,
441 implementing such studies is difficult and expensive, and collecting sufficient sample data to
442 support robust and generalizable models is generally not possible. Reflecting these challenges,
443 results from a meta-analysis of warming studies showed that phenological changes observed in

444 such experiments do not replicate the magnitude of phenological responses to natural variation in
445 air temperature observed in natural systems (Wolkovich et al., 2012).

446 Data-driven models like the CDSOM are not a panacea, but they do resolve several of the
447 issues discussed above. In addition to addressing the three limitations identified by Clark et al.
448 (2014a, 2014b), functional relationships among control variables in CDSOM are entirely
449 estimated from data. Hence the CDSOM avoids issues related to misspecification of functional
450 relationships that are inherent to conventional models. Further, by exploiting time series of
451 remote sensing observations collected over large areas that span nearly two decades, the
452 CDSOM results presented here capture and reflect a much broader range of climate regimes and
453 climate variability than is generally possible using designed experiments. Indeed, we posit that
454 natural variability captured through interannual variability in climate over large geographic
455 scales provides an important and useful strategy for characterizing and understanding the
456 sensitivity of plant phenology to climate change (Friedl et al., 2014).

457 Moreover, and perhaps most importantly, while the patterns presented in Figs. 4-7 are
458 superficially consistent with results from previous studies suggesting that the timing of spring
459 greenup in deciduous forests has become less sensitive to thermal forcing and that the so-called
460 ‘temperature sensitive period’ of temperate and boreal trees is changing (Fu et al., 2019, 2015;
461 Piao et al., 2017). We suggest that this inference may be spurious. Specifically, results from the
462 CDSOM show that thermal forcing control on the timing of greenup is heterogeneous and
463 exhibits weak covariance with pre-season period. Hence, apparent decreases in temperature
464 sensitivity actually reflect shorter pre-season periods with increased photoperiod control (Keenan
465 et al., 2019). Stated another way, as the climate warms, higher temperatures tend to increase the
466 relative importance of photoperiod, while dependence on temperature has remained relatively

467 constant. Further, in regions where mean annual temperature is below ~ 10 °C, which
468 encompasses a significant proportion of the temperate zone and all of the boreal zone,
469 photoperiod control is modest and thermal forcing is clearly the dominant control. Indeed, our
470 results suggest that the biogeographic range in which the relative importance of photoperiod
471 control is increasing is restricted to locations with mean annual temperatures between ~ 8 - 10 °C,
472 and hence, is relatively narrow.

473 The simplest explanation for why photoperiod control varies geographically is provided by
474 the “law of the minimum”, which states that plant growth is controlled by the scarcest resource
475 rather than by the total resources available (Liebig et al., 1841). Our results are, to a first order,
476 consistent with this law. In cold regions (i.e., identified here as regions where mean annual
477 temperature is less than ~ 10 °C; Fig. 5), temperature is the primary limiting factor that controls
478 the timing of greenup. In warmer regions where temperature is less limiting, light (or moisture)
479 becomes the primary limiting resource. Invoking a similar argument, Park et al. (2019) suggest
480 that extensive areas of high-latitude ecosystems that were previously constrained by temperature
481 are becoming more sensitive to photoperiod. Further, the results from our study are consistent
482 with recent experimental results from Zohner et al. (2016), who concluded that springtime
483 phenology in deciduous trees at lower latitudes tended to depend more strongly on photoperiod,
484 while species at high latitudes leafed out independent of photoperiod. Hence our results are
485 consistent with both long-established and more recent ecological literature.

486 Lastly, it is important to note several limitations of the current study. First, rather than
487 modeling the role of chilling in controlling spring greenup using continuous (i.e., daily) forcing
488 (Hänninen et al., 2019; Murray et al., 1989), the CDSOM uses chilling units, which provide an
489 accumulated measure chilling requirements. This suggests that the role of the chilling units may

490 not be fully accounted for in this study, and may explain the relatively minor role of chilling
491 units in predicting the timing of spring greenup that we observed in this study (Fig. 4c and d)
492 (c.f., Heide and Prestrud, 2005; Laube et al., 2014). Second, to capture the effect of thermal
493 forcing, the CDSOM used daily mean temperature as opposed to other measures of thermal
494 forcing such as daily maximum and minimum temperature, which some studies have suggested
495 may be better predictors. However, results from CDSOM using daily maximum and minimum
496 temperatures as inputs did not show significant differences from results based on daily mean
497 temperatures (not shown), and more generally, results from studies that have explored this
498 question are somewhat inconsistent (c.f., Huang et al., 2020; Piao et al., 2015; Shen et al., 2018).
499 That said, because continuous development models are explicitly designed to capture the effects
500 of short-term variability in forcing variables, selection of optimal metrics to this variability is
501 clearly important and merits more investigation.

502

503 **5. Conclusions**

504 Changes in springtime phenology are among the most obvious and observable responses of
505 organisms to climate change, but the mechanisms behind these changes are poorly understood
506 (Parmesan and Yohe, 2003; Piao et al., 2019). By directly estimating and mapping the
507 geographic dependence of greenup on photoperiod and thermal forcing, results from this study
508 elucidate how the nature and magnitude bioclimatic control on spring phenology depend on
509 geography and climate, and provide a novel and nuanced explanation for why the temperature
510 sensitivity of deciduous forests appears to be decreasing. Specifically, our results indicate that
511 apparent changes in temperature sensitivity may reflect a misinterpretation of the data, and where
512 present, observed decreases actually reflect increased dependence on photoperiod. The results

513 also help to clarify the mechanisms behind observed changes and have important implications
514 for a variety of ecological processes, such as the role of safety mechanisms that are widely
515 ascribed to photoperiod constraints on spring phenology (Körner and Basler, 2010). For example,
516 Fig. 5 shows that the relative importance of photoperiod decreases as mean annual temperature
517 decreases, which suggests that safety mechanisms related to photoperiod provide only modest
518 protection in colder climates (Richardson et al., 2018a). More generally, our results support the
519 argument posited by Zohner et al. (2016) who reported that tree species with strong photoperiod
520 control on leaf-out tend to be located in warmer regions, and challenge the idea that photoperiod
521 provides a safeguard against early leaf emergence in temperate woody species.

522

523 **Acknowledgements**

524 This research was funded by the MacroSystems Biology Program of National Science
525 Foundation (Grant numbers EF 1702627 and 1702697). ADR acknowledges support from NSF's
526 LTER program through DEB-1637685 and and DEB-1832210.

527

528 **Author contributions**

529 M.M. and M.A.F designed the analysis and led the drafting of the manuscript. M.M. and B.S.
530 developed the model. MM. performed the analysis. B.S. and A.D.R. contributed analysis ideas
531 and participated in drafting the manuscript.

532

533 **Competing interests**

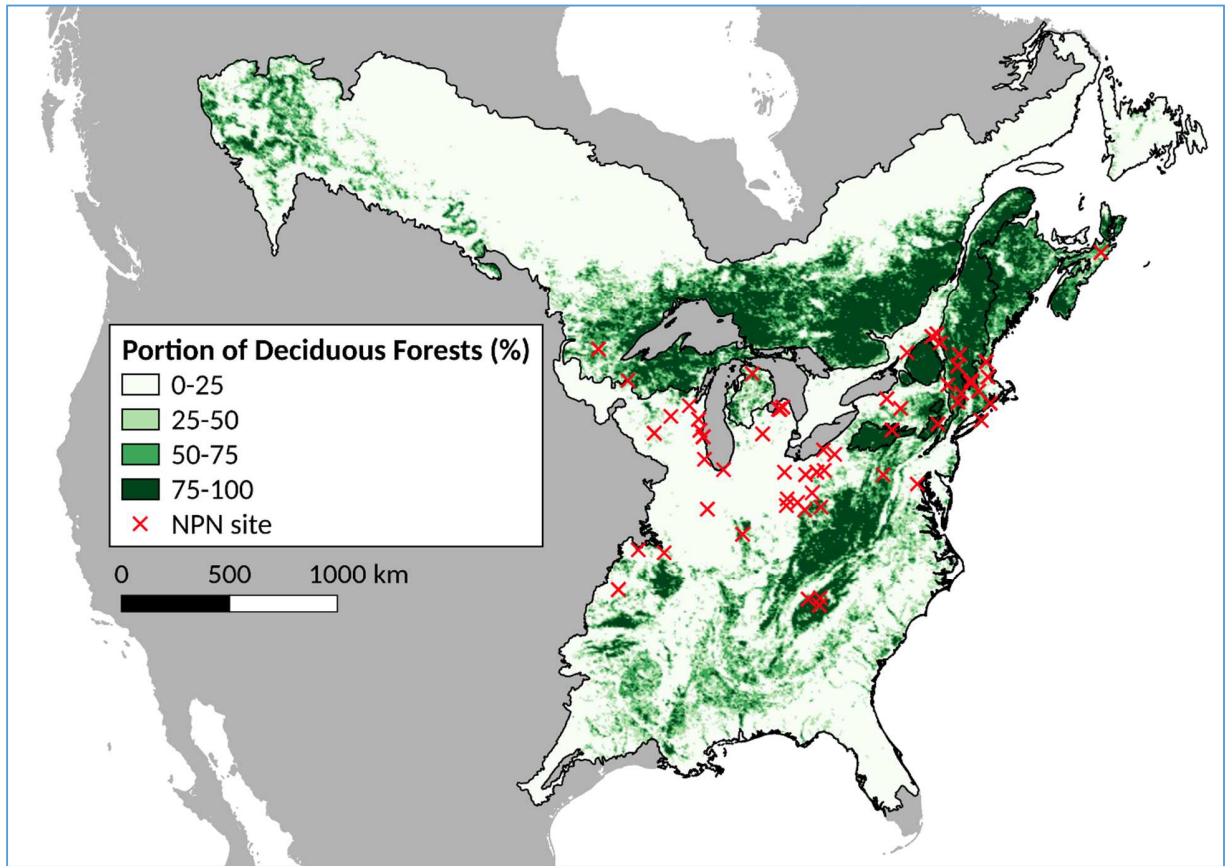
534 The authors declare no competing interests.

535 **Appendix**

536 **Table A1.** Models descriptions

Model	Model type	Variables	Main characteristics & Statistical assumptions of the model
CDSOM	Date-driven	$h; \delta h; h_{max}; X; T; L; CU; \beta; P; \kappa; \lambda; Y; T_b$	Phenological development responses continuously to variations in environmental controls at daily time step throughout pre-season period; Invoking no assumptions about functional relationships between control variables
TT	Knowledge-driven	$F^*; S_f; T; T_b$	Greenup onset occurs when accumulated forcing reaches a critical threshold, which solely relies only on thermal forcing with no additional factors
PTT	Knowledge-driven	$F^*; S_f; T; T_b; L$	Greenup onset occurs when accumulated forcing reaches a critical threshold, but the rate of thermal forcing is regulated by photoperiod
M1	Knowledge-driven	$F^*; S_f; T; T_b; L; k$	Greenup onset occurs when accumulated forcing reaches a critical threshold, but the rate of thermal forcing is regulated by photoperiod as an exponential
AT	Knowledge-driven	$F^*; NCD; a; b; c$	Greenup onset occurs when accumulated forcing reaches a critical threshold, but the rate of thermal forcing is regulated by the number of chilling days

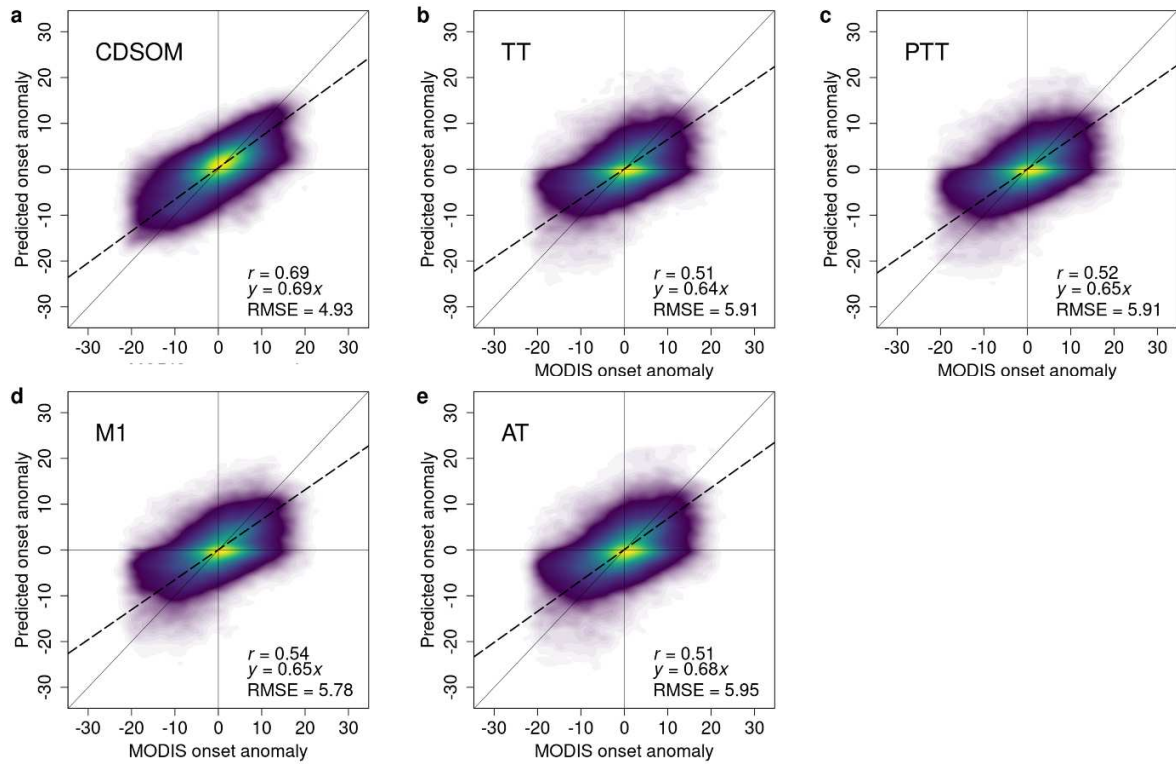
537 CDSOM: Continuous Development Spring Onset Model; TT: Thermal Time model (TT); PTT: Photo-Thermal Time model (PTT);
538 M1: Exponential Photo-Thermal Time model (M1); AT: Alternating model; h : latent state; δh : daily latent state increment; h_{max} :
539 theoretical final state of h ; X : matrix of predictor variables T , L , and CU (daily mean temperature, day-length, and chilling units,
540 respectively); β : vector of estimated model coefficient for T , L , and CU; P : probability that greenup onset occurs; κ and λ : intercept
541 and slope for logit transformation, respectively; Y : Bernoulli trial indicating whether or not greenup onset has occurred; T_b : base
542 temperature for chilling requirement; F^* : critical threshold that spring greenup onset occurs when the state of forcing (S_f) reaches it; k :
543 exponential coefficient for M1; NCD: number of chilling days; estimated constants for AT



545

546 **Fig. A1.** Map of the study area. Extents of the US EPA Northern Forest and Eastern Temperate
547 Forest ecoregions, along with the proportion 500 m MODIS pixels labeled as deciduous forests
548 in each grid cell according to the Collection 6 MODIS Land Cover Type product. Red crosses
549 show the USA-National Phenology Network site locations where lilac data are collected. Note
550 that because the MODIS Land Cover Type product uses a threshold of 60% cover to define
551 forest classes, the map shown in Fig. A1 modestly over-represents the actual proportion of
552 deciduous forest cover.

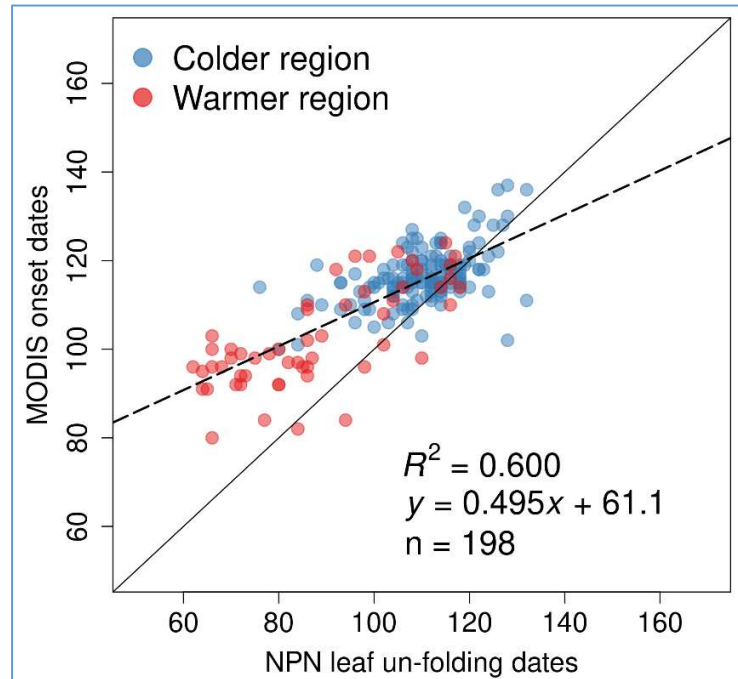
553



554

555 **Fig. A2.** Relationship between anomalies in MODIS onset dates and anomalies in model-
 556 predicted onset dates. Panels (a)-(e) show results for the Continuous Development Spring Onset
 557 Model (CDSOM), the thermal time model (TT), the photo-thermal time model (PTT), the
 558 exponential photo-thermal time model (M1), and the alternating model (AT), respectively.
 559 Dashed lines and correlation coefficients (r) show the results from standard major axis regression.

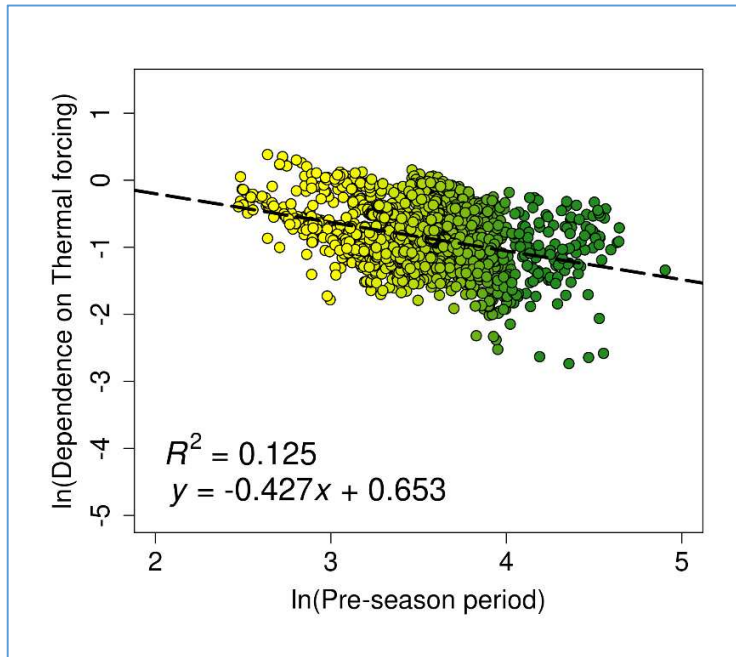
560



561

562 **Fig. A3.** Relationship between MODIS greenup dates and leaf unfolding dates from the USA-
 563 NPN cloned lilac dataset. The colder (red dots) and warmer (blue dots) sites are divided based on
 564 mean annual temperature (i.e., colder ≤ 10 °C; warmer > 10 °C). n (= 198) is different from the
 565 total number of USA-NPN leaf unfolding dates ($n = 254$) due to cases where no MODIS dates
 566 were available because the lilac site was not located in a location dominated by deciduous or
 567 mixed forest at the scale of MODIS pixels.

568



569

570 **Fig. A4.** Relationship between pre-season period length and dependence on thermal forcing.

571

572 **References**

- 573 Abercrombie, S.P., Friedl, M.A., 2016. Improving the Consistency of Multitemporal Land Cover Maps
 574 Using a Hidden Markov Model. *IEEE Transactions on Geoscience and Remote Sensing* 54, 703–
 575 713. <https://doi.org/10.1109/TGRS.2015.2463689>
- 576 Basler, D., 2016. Evaluating phenological models for the prediction of leaf-out dates in six temperate tree
 577 species across central Europe. *Agricultural and Forest Meteorology* 217, 10–21.
 578 <https://doi.org/10.1016/j.agrformet.2015.11.007>
- 579 Basler, D., Körner, C., 2012. Photoperiod sensitivity of bud burst in 14 temperate forest tree species.
 580 *Agricultural and Forest Meteorology* 165, 73–81. <https://doi.org/10.1016/j.agrformet.2012.06.001>
- 581 Blümel, K., Chmielewski, F.-M., 2012. Shortcomings of classical phenological forcing models and a way
 582 to overcome them. *Agricultural and Forest Meteorology* 164, 10–19.
 583 <https://doi.org/10.1016/j.agrformet.2012.05.001>
- 584 Bolton, D.K., Gray, J.M., Melaas, E.K., Moon, M., Eklundh, L., Friedl, M.A., 2020. Continental-scale
 585 land surface phenology from harmonized Landsat 8 and Sentinel-2 imagery. *Remote Sensing of*
 586 *Environment* 240, 111685. <https://doi.org/10.1016/j.rse.2020.111685>
- 587 Cannell, M.G.R., Smith, R.I., 1983. Thermal Time, Chill Days and Prediction of Budburst in *Picea*
 588 *sitchensis*. *Journal of Applied Ecology* 20, 951–963. <https://doi.org/10.2307/2403139>
- 589 Chuine, I., Bonhomme, M., Legave, J.-M., García de Cortázar-Atauri, I., Charrier, G., Lacoite, A.,
 590 Améglio, T., 2016. Can phenological models predict tree phenology accurately in the future? The
 591 unrevealed hurdle of endodormancy break. *Glob Change Biol* 22, 3444–3460.
 592 <https://doi.org/10.1111/gcb.13383>
- 593 Chuine, I., Cour, P., Rousseau, D.D., 1999. Selecting models to predict the timing of flowering of
 594 temperate trees: implications for tree phenology modelling. *Plant, Cell & Environment* 22, 1–13.
 595 <https://doi.org/10.1046/j.1365-3040.1999.00395.x>
- 596 Chuine, I., Régnière, J., 2017. Process-Based Models of Phenology for Plants and Animals. *Annu. Rev.*
 597 *Ecol. Evol. Syst.* 48, 159–182. <https://doi.org/10.1146/annurev-ecolsys-110316-022706>
- 598 Clark, J.S., Melillo, J., Mohan, J., Salk, C., 2014a. The seasonal timing of warming that controls onset of
 599 the growing season. *Global Change Biology* 20, 1136–1145. <https://doi.org/10.1111/gcb.12420>
- 600 Clark, J.S., Salk, C., Melillo, J., Mohan, J., 2014b. Tree phenology responses to winter chilling, spring
 601 warming, at north and south range limits. *Functional Ecology* 28, 1344–1355.
 602 <https://doi.org/10.1111/1365-2435.12309>
- 603 Črepinšek, Z., Kajfež-Bogataj, L., Bergant, K., 2006. Modelling of weather variability effect on
 604 fitophenology. *Ecological Modelling, Special Issue on the Fourth European Conference on*
 605 *Ecological Modelling* 194, 256–265. <https://doi.org/10.1016/j.ecolmodel.2005.10.020>
- 606 Friedl, M.A., Gray, J.M., Melaas, E.K., Richardson, A.D., Hufkens, K., Keenan, T.F., Amey Bailey,
 607 O’Keefe, J., 2014. A tale of two springs: using recent climate anomalies to characterize the
 608 sensitivity of temperate forest phenology to climate change. *Environ. Res. Lett.* 9, 054006.
 609 <https://doi.org/10.1088/1748-9326/9/5/054006>
- 610 Fu, Y.H., Geng, X., Hao, F., Vitasse, Y., Zohner, C.M., Zhang, X., Zhou, X., Yin, G., Peñuelas, J., Piao,
 611 S., Janssens, I.A., 2019. Shortened temperature-relevant period of spring leaf-out in temperate-
 612 zone trees. *Global Change Biology* 25, 4282–4290. <https://doi.org/10.1111/gcb.14782>
- 613 Fu, Y.H., Zhao, H., Piao, S., Peaucelle, M., Peng, S., Zhou, G., Ciais, P., Huang, M., Menzel, A.,
 614 Peñuelas, J., Song, Y., Vitasse, Y., Zeng, Z., Janssens, I.A., 2015. Declining global warming
 615 effects on the phenology of spring leaf unfolding. *Nature* 526, 104–107.
 616 <https://doi.org/10.1038/nature15402>
- 617 Gray, J., Sulla-Menashe, D., Friedl, M.A., 2019. User Guide to Collection 6 MODIS Land Cover
 618 Dynamics (MCD12Q2) Product. <https://doi.org/10.5067/MODIS/MCD12Q2.006>
- 619 Güsewell, S., Furrer, R., Gehrig, R., Pietragalla, B., 2017. Changes in temperature sensitivity of spring
 620 phenology with recent climate warming in Switzerland are related to shifts of the preseason.
 621 *Global Change Biology* 23, 5189–5202. <https://doi.org/10.1111/gcb.13781>

622 Hänninen, H., Kramer, K., Tanino, K., Zhang, R., Wu, J., Fu, Y.H., 2019. Experiments Are Necessary in
623 Process-Based Tree Phenology Modelling. *Trends in Plant Science* 24, 199–209.
624 <https://doi.org/10.1016/j.tplants.2018.11.006>

625 Heide, O.M., Prestrud, A.K., 2005. Low temperature, but not photoperiod, controls growth cessation and
626 dormancy induction and release in apple and pear. *Tree Physiology* 25, 109–114.
627 <https://doi.org/10.1093/treephys/25.1.109>

628 Huang, Y., Jiang, N., Shen, M., Guo, L., 2020. Effect of pre-season diurnal temperature range on the start
629 of vegetation growing season in the Northern Hemisphere. *Ecological Indicators* 112, 106161.
630 <https://doi.org/10.1016/j.ecolind.2020.106161>

631 Hufkens, K., Basler, D., Milliman, T., Melaas, E.K., Richardson, A.D., 2018. An integrated phenology
632 modelling framework in R. *Methods in Ecology and Evolution* 9, 1276–1285.
633 <https://doi.org/10.1111/2041-210X.12970>

634 Hunter, A.F., Lechowicz, M.J., 1992. Predicting the Timing of Budburst in Temperate Trees. *Journal of*
635 *Applied Ecology* 29, 597–604. <https://doi.org/10.2307/2404467>

636 Jackson, S.D., 2009. Plant responses to photoperiod. *New Phytologist* 181, 517–531.
637 <https://doi.org/10.1111/j.1469-8137.2008.02681.x>

638 Keenan, T.F., Gray, J., Friedl, M.A., Toomey, M., Bohrer, G., Hollinger, D.Y., Munger, J.W., O’Keefe, J.,
639 Schmid, H.P., Wing, I.S., Yang, B., Richardson, A.D., 2014. Net carbon uptake has increased
640 through warming-induced changes in temperate forest phenology. *Nature Climate Change* 4,
641 598–604. <https://doi.org/10.1038/nclimate2253>

642 Keenan, T.F., Richardson, A.D., Hufkens, K., 2019. On quantifying the apparent temperature sensitivity
643 of plant phenology. *New Phytol* 16114. <https://doi.org/10.1111/nph.16114>

644 Körner, C., Basler, D., 2010. Phenology Under Global Warming. *Science* 327, 1461–1462.
645 <https://doi.org/10.1126/science.1186473>

646 Laube, J., Sparks, T.H., Estrella, N., Höfler, J., Ankerst, D.P., Menzel, A., 2014. Chilling outweighs
647 photoperiod in preventing precocious spring development. *Global Change Biology* 20, 170–182.
648 <https://doi.org/10.1111/gcb.12360>

649 Liu, Q., Fu, Y.H., Liu, Y., Janssens, I.A., Piao, S., 2017. Simulating the onset of spring vegetation growth
650 across the Northern Hemisphere. *Global Change Biology* 24, 1342–1356.
651 <https://doi.org/10.1111/gcb.13954>

652 Masle, J., Doussinault, G., Farquhar, G.D., Sun, B., 1989. Foliar stage in wheat correlates better to
653 photothermal time than to thermal time. *Plant, Cell & Environment* 12, 235–247.
654 <https://doi.org/10.1111/j.1365-3040.1989.tb01938.x>

655 Melaas, E.K., Richardson, A.D., Friedl, M.A., Dragoni, D., Gough, C.M., Herbst, M., Montagnani, L.,
656 Moors, E., 2013. Using FLUXNET data to improve models of springtime vegetation activity
657 onset in forest ecosystems. *Agricultural and Forest Meteorology* 171–172, 46–56.
658 <https://doi.org/10.1016/j.agrformet.2012.11.018>

659 Melaas, E.K., Sulla-Menashe, D., Friedl, M.A., 2018. Multidecadal Changes and Interannual Variation in
660 Springtime Phenology of North American Temperate and Boreal Deciduous Forests. *Geophysical*
661 *Research Letters* 45, 2679–2687. <https://doi.org/10.1002/2017GL076933>

662 Menzel, A., Sparks, T.H., Estrella, N., Koch, E., Aasa, A., Ahas, R., Alm-Kübler, K., Bissolli, P.,
663 Braslavská, O., Briede, A., Chmielewski, F.M., Crepinsek, Z., Curnel, Y., Dahl, Å., Defila, C.,
664 Donnelly, A., Filella, Y., Jatzczak, K., Måge, F., Mestre, A., Nordli, Ø., Peñuelas, J., Pirinen, P.,
665 Remišová, V., Scheffinger, H., Striz, M., Susnik, A., Vliet, A.J.H.V., Wielgolaski, F.-E., Zach, S.,
666 Zust, A., 2006. European phenological response to climate change matches the warming pattern.
667 *Global Change Biology* 12, 1969–1976. <https://doi.org/10.1111/j.1365-2486.2006.01193.x>

668 Migliavacca, M., Sonntag, O., Keenan, T.F., Cescatti, A., O’Keefe, J., Richardson, A.D.,
669 2012. On the uncertainty of phenological responses to climate change, and implications for a
670 terrestrial biosphere model. *Biogeosciences* 9, 2063–2083. [https://doi.org/10.5194/bg-9-2063-](https://doi.org/10.5194/bg-9-2063-2012)
671 2012

672 Montgomery, R.A., Rice, K.E., Stefanski, A., Rich, R.L., Reich, P.B., 2020. Phenological responses of
673 temperate and boreal trees to warming depend on ambient spring temperatures, leaf habit, and
674 geographic range. *Proc Natl Acad Sci USA* 201917508. <https://doi.org/10.1073/pnas.1917508117>

675 Moon, M., Li, D., Liao, W., Rigden, A.J., Friedl, M.A., 2020. Modification of surface energy balance
676 during springtime: The relative importance of biophysical and meteorological changes.
677 *Agricultural and Forest Meteorology* 284, 107905.
678 <https://doi.org/10.1016/j.agrformet.2020.107905>

679 Moon, M., Zhang, X., Henebry, G.M., Liu, L., Gray, J.M., Melaas, E.K., Friedl, M.A., 2019. Long-term
680 continuity in land surface phenology measurements: A comparative assessment of the MODIS
681 land cover dynamics and VIIRS land surface phenology products. *Remote Sensing of
682 Environment* 226, 74–92. <https://doi.org/10.1016/j.rse.2019.03.034>

683 Murray, M.B., Cannell, M.G.R., Smith, R.I., 1989. Date of Budburst of Fifteen Tree Species in Britain
684 Following Climatic Warming. *Journal of Applied Ecology* 26, 693–700.
685 <https://doi.org/10.2307/2404093>

686 Park, T., Chen, C., Macias-Fauria, M., Tømmervik, H., Choi, S., Winkler, A., Bhatt, U.S., Walker, D.A.,
687 Piao, S., Brovkin, V., Nemani, R.R., Myneni, R.B., 2019. Changes in timing of seasonal peak
688 photosynthetic activity in northern ecosystems. *Glob Change Biol* gcb.14638.
689 <https://doi.org/10.1111/gcb.14638>

690 Parmesan, C., Yohe, G., 2003. A globally coherent fingerprint of climate change impacts across natural
691 systems. *Nature* 421, 37–42. <https://doi.org/10.1038/nature01286>

692 Peñuelas, J., Rutishauser, T., Filella, I., 2009. Phenology Feedbacks on Climate Change. *Science* 324,
693 887–888. <https://doi.org/10.1126/science.1173004>

694 Piao, S., Liu, Q., Chen, A., Janssens, I.A., Fu, Y., Dai, J., Liu, L., Lian, X., Shen, M., Zhu, X., 2019. Plant
695 phenology and global climate change: current progresses and challenges. *Global Change Biology*.
696 <https://doi.org/10.1111/gcb.14619>

697 Piao, S., Liu, Z., Wang, T., Peng, S., Ciais, P., Huang, M., Ahlstrom, A., Burkhardt, J.F., Chevallier, F.,
698 Janssens, I.A., Jeong, S.-J., Lin, X., Mao, J., Miller, J., Mohammat, A., Myneni, R.B., Peñuelas,
699 J., Shi, X., Stohl, A., Yao, Y., Zhu, Z., Tans, P.P., 2017. Weakening temperature control on the
700 interannual variations of spring carbon uptake across northern lands. *Nature Climate Change* 7,
701 359–363. <https://doi.org/10.1038/nclimate3277>

702 Piao, S., Tan, J., Chen, A., Fu, Y.H., Ciais, P., Liu, Q., Janssens, I.A., Vicca, S., Zeng, Z., Jeong, S.-J., Li,
703 Y., Myneni, R.B., Peng, S., Shen, M., Peñuelas, J., 2015. Leaf onset in the northern hemisphere
704 triggered by daytime temperature. *Nature Communications* 6, 6911.
705 <https://doi.org/10.1038/ncomms7911>

706 Qiu, T., Song, C., Clark, J.S., Seyednasrollah, B., Rathnayaka, N., Li, J., 2020. Understanding the
707 continuous phenological development at daily time step with a Bayesian hierarchical space-time
708 model: impacts of climate change and extreme weather events. *Remote Sensing of Environment*
709 247, 111956. <https://doi.org/10.1016/j.rse.2020.111956>

710 Richardson, A.D., Hufkens, K., Milliman, T., Aubrecht, D.M., Furze, M.E., Seyednasrollah, B.,
711 Krassovski, M.B., Latimer, J.M., Nettles, W.R., Heiderman, R.R., Warren, J.M., Hanson, P.J.,
712 2018a. Ecosystem warming extends vegetation activity but heightens vulnerability to cold
713 temperatures. *Nature*. <https://doi.org/10.1038/s41586-018-0399-1>

714 Richardson, A.D., Hufkens, K., Milliman, T., Frolking, S., 2018b. Intercomparison of phenological
715 transition dates derived from the PhenoCam Dataset V1.0 and MODIS satellite remote sensing.
716 *Scientific Reports* 8, 5679. <https://doi.org/10.1038/s41598-018-23804-6>

717 Richardson, A.D., Keenan, T.F., Migliavacca, M., Ryu, Y., Sonnentag, O., Toomey, M., 2013. Climate
718 change, phenology, and phenological control of vegetation feedbacks to the climate system.
719 *Agricultural and Forest Meteorology* 169, 156–173.
720 <https://doi.org/10.1016/j.agrformet.2012.09.012>

721 Rosemartin, A.H., Denny, E.G., Weltzin, J.F., Lee Marsh, R., Wilson, B.E., Mehdipoor, H., Zurita-Milla,
722 R., Schwartz, M.D., 2015. Lilac and honeysuckle phenology data 1956–2014. *Scientific Data* 2,
723 150038. <https://doi.org/10.1038/sdata.2015.38>

724 Schewe, J., Gosling, S.N., Reyer, C., Zhao, F., Ciais, P., Elliott, J., Francois, L., Huber, V., Lotze, H.K.,
725 Seneviratne, S.I., van Vliet, M.T.H., Vautard, R., Wada, Y., Breuer, L., Büchner, M., Carozza,
726 D.A., Chang, J., Coll, M., Deryng, D., de Wit, A., Eddy, T.D., Folberth, C., Frieler, K., Friend,
727 A.D., Gerten, D., Gudmundsson, L., Hanasaki, N., Ito, A., Khabarov, N., Kim, H., Lawrence, P.,
728 Morfopoulos, C., Müller, C., Müller Schmied, H., Orth, R., Ostberg, S., Pokhrel, Y., Pugh,
729 T.A.M., Sakurai, G., Satoh, Y., Schmid, E., Stacke, T., Steenbeek, J., Steinkamp, J., Tang, Q.,
730 Tian, H., Tittensor, D.P., Volkholz, J., Wang, X., Warszawski, L., 2019. State-of-the-art global
731 models underestimate impacts from climate extremes. *Nature Communications* 10, 1005.
732 <https://doi.org/10.1038/s41467-019-08745-6>

733 Schwartz, M.D., Ahas, R., Aasa, A., 2006. Onset of spring starting earlier across the Northern
734 Hemisphere. *Global Change Biology* 12, 343–351. <https://doi.org/10.1111/j.1365-2486.2005.01097.x>

735

736 Senf, C., Pflugmacher, D., Heurich, M., Krueger, T., 2017. A Bayesian hierarchical model for estimating
737 spatial and temporal variation in vegetation phenology from Landsat time series. *Remote Sensing*
738 of Environment 194, 155–160. <https://doi.org/10.1016/j.rse.2017.03.020>

739 Seyednasrollah, B., Swenson, J.J., Domec, J.-C., Clark, J.S., 2018. Leaf phenology paradox: Why
740 warming matters most where it is already warm. *Remote Sensing of Environment* 209, 446–455.
741 <https://doi.org/10.1016/j.rse.2018.02.059>

742 Seyednasrollah, B., Young, A.M., Li, X., Milliman, T., Ault, T., Frolking, S., Friedl, M., Richardson,
743 A.D., 2020. Sensitivity of Deciduous Forest Phenology to Environmental Drivers: Implications
744 for Climate Change Impacts Across North America. *Geophys. Res. Lett.* 47.
745 <https://doi.org/10.1029/2019GL086788>

746 Shen, X., Liu, B., Henderson, M., Wang, L., Wu, Z., Wu, H., Jiang, M., Lu, X., 2018. Asymmetric effects
747 of daytime and nighttime warming on spring phenology in the temperate grasslands of China.
748 *Agricultural and Forest Meteorology* 259, 240–249.
749 <https://doi.org/10.1016/j.agrformet.2018.05.006>

750 Su, Y.-S., Yajima, M., 2015. R2jags: Using R to Run “JAGS”.

751 Sulla-Menashe, D., Gray, J.M., Abercrombie, S.P., Friedl, M.A., 2019. Hierarchical mapping of annual
752 global land cover 2001 to present: The MODIS Collection 6 Land Cover product. *Remote*
753 *Sensing of Environment* 222, 183–194. <https://doi.org/10.1016/j.rse.2018.12.013>

754 Thornton, P.E., Thornton, M.M., Mayer, B.W., Wei, Y., Devarakonda, R., Vose, R.S., Cook, R.B., 2017.
755 Daymet: Daily Surface Weather Data on a 1-km Grid for North America, Version 3.
756 <https://doi.org/10.3334/ORNLDAAAC/1328>

757 Walther, G.-R., Post, E., Convey, P., Menzel, A., Parmesan, C., Beebee, T.J.C., Fromentin, J.-M., Hoegh-
758 Guldberg, O., Bairlein, F., 2002. Ecological responses to recent climate change. *Nature* 416, 389–
759 395. <https://doi.org/10.1038/416389a>

760 Wenden, B., Mariadassou, M., Chmielewski, F.-M., Vitasse, Y., 2020. Shifts in the temperature-sensitive
761 periods for spring phenology in European beech and pedunculate oak clones across latitudes and
762 over recent decades. *Global Change Biology* 26, 1808–1819. <https://doi.org/10.1111/gcb.14918>

763 Wolkovich, E.M., Cook, B.I., Allen, J.M., Crimmins, T.M., Betancourt, J.L., Travers, S.E., Pau, S.,
764 Regetz, J., Davies, T.J., Kraft, N.J.B., Ault, T.R., Bolmgren, K., Mazer, S.J., McCabe, G.J.,
765 McGill, B.J., Parmesan, C., Salamin, N., Schwartz, M.D., Cleland, E.E., 2012. Warming
766 experiments underpredict plant phenological responses to climate change. *Nature* 485, 494–497.
767 <https://doi.org/10.1038/nature11014>

768 Zhang, X., Liu, L., Liu, Y., Jayavelu, S., Wang, J., Moon, M., Henebry, G.M., Friedl, M.A., Schaaf, C.B.,
769 2018. Generation and evaluation of the VIIRS land surface phenology product. *Remote Sensing*
770 of Environment 216, 212–229. <https://doi.org/10.1016/j.rse.2018.06.047>

771 Zohner, C.M., Benito, B.M., Svenning, J.-C., Renner, S.S., 2016. Day length unlikely to constrain
772 climate-driven shifts in leaf-out times of northern woody plants. *Nature Climate Change* 6, 1120–
773 1123. <https://doi.org/10.1038/nclimate3138>
774

775

776 **List of Figure Captions**

777 **Fig. 1.** Model results for a randomly selected grid cell. (a) Relationship between the greenup
778 onset dates from MODIS and onset dates estimated by the model. (b) The distribution of model
779 coefficients for each control variable (i.e., the relative dependence on each climate control;
780 Therm.: thermal forcing; Photo.: photoperiod; Chill.: chilling units). (c) Time series of the latent
781 state (red line) and the length of the pre-season (identified by the horizontal arrow). In panel (a),
782 each dot (total $n = 100$) represents an individual pixel-year sampled from the grid cell comprised
783 of 10 by 10 MODIS pixels across 17 years of the study period (i.e., 100 out of the total 1,700
784 pixel-years).

785

786 **Fig. 2.** Continuous Development Spring Onset Model (CDSOM) performance. (a) Geographic
787 variation in model root-mean-square errors (RMSE) between greenup onset dates observed from
788 MODIS and onset dates predicted by the CDSOM model. (b) Boxplots showing the distribution
789 of RMSEs for the CDSOM model and four widely used conventional spring greenup models.
790 M1: The exponential photo-thermal time model; PTT: The photo-thermal time model; TT: The
791 thermal time model; AT: The alternating model. In panel (b), boxplots are presented in
792 increasing order of magnitude with respect to mean RMSE.

793

794 **Fig. 3.** RMSE results across models for anomalous years. (a) Boxplots of RMSEs for each model
795 for 2010 and 2012. (b) Boxplots showing increase in RMSEs for model predictions for all years
796 versus anomalous years (i.e., RMSEs for 2010 and 2012 – RMSEs for 2001-2017) at each grid
797 cell. CDSOM: continuous development spring onset model; M1: The exponential photo-thermal

798 time model; PTT: The photo-thermal time model; TT: The thermal time model; AT: The
799 alternating model. Boxplots are presented in increasing order of magnitude with respect to mean
800 RMSE.

801

802 **Fig. 4.** Geographic variation in the dependence of spring greenup onset date to: (a) thermal
803 forcing, (b) photoperiod, and (c) chilling units. In panel (d), boxplots show the distribution of
804 model coefficients for each control variable during the pre-season period prior to leaf emergence
805 in Northern Forests (blue) versus Eastern Temperate Forests (red). Differences between the
806 means in both cases are statistically significant ($p < 0.001$).

807

808 **Fig. 5.** Relative importance (*RI*) of thermal forcing versus photoperiod. Circles in red and blue
809 show locations where thermal forcing and photoperiod, respectively, exert stronger control on
810 the timing of spring greenup; purple circles identify locations where the magnitude of thermal
811 forcing and photoperiod are roughly equivalent. The size of each circle is proportional to the
812 magnitude of *RI* in each cell.

813

814 **Fig. 6.** Dependence of cloned lilac leaf unfolding date on thermal forcing and photoperiod, and
815 relative importance (*RI*). 254 total leaf unfolding dates from cloned lilac were divided into two
816 groups based on mean annual temperature (≤ 10 °C, $n = 182$; > 10 °C, $n = 72$). The left panel
817 plots the mean dependence of leaf unfolding on thermal forcing and photoperiod estimated by
818 the CDSOM. The right panel plots the mean *RI* in each group. Positive *RI* indicates stronger
819 control by thermal forcing relative to photoperiod. Vertical lines show ± 1 standard deviation.

820

821 **Fig. 7.** Variation in pre-season period and the relationship between greenup dependence on
822 photoperiod and length of pre-season period. (a) Geographic pattern in pre-season period, and (b)
823 log-log relationship between the dependence of greenup on photoperiod and the length of the
824 pre-season period.

825

826 **Fig. A1.** Map of the study area. Extents of the US EPA Northern Forest and Eastern Temperate
827 Forest ecoregions, along with the proportion 500 m MODIS pixels labeled as deciduous forests
828 in each grid cell according to the Collection 6 MODIS Land Cover Type product. Red crosses
829 show the USA-National Phenology Network site locations where lilac data are collected. Note
830 that because the MODIS Land Cover Type product uses a threshold of 60% cover to define
831 forest classes, the map shown in Fig. A1 modestly over-represents the actual proportion of
832 deciduous forest cover.

833

834 **Fig. A2.** Relationship between anomalies in MODIS onset dates and anomalies in model-
835 predicted onset dates. Panels (a)-(e) show results for the Continuous Development Spring Onset
836 Model (CDSOM), the thermal time model (TT), the photo-thermal time model (PTT), the
837 exponential photo-thermal time model (M1), and the alternating model (AT), respectively.
838 Dashed lines and correlation coefficients (r) show the results from standard major axis regression.

839

840 **Fig. A3.** Relationship between MODIS greenup dates and leaf unfolding dates from the USA-
841 NPN cloned lilac dataset. The colder (red dots) and warmer (blue dots) sites are divided based on
842 mean annual temperature (i.e., colder ≤ 10 °C; warmer > 10 °C). n (= 198) is different from the
843 total number of USA-NPN leaf unfolding dates ($n = 254$) due to cases where no MODIS dates
844 were available because the lilac site was not located in a location dominated by deciduous or
845 mixed forest at the scale of MODIS pixels.

846

847 **Fig. A4.** Relationship between pre-season period length and dependence on thermal forcing.

848